Preprints.org

Article

Not peer-reviewed version

Microstructures and Antioxidation of W Self-Passivating Alloys: Synergistic Effect of Yttrium and Milling Time

Shijie Chen , Shirong Zhang , Rui Wang , Chao Ye , Lihong Xue * , Shengming Yin , Youwei Yan , Qilai Zhou

Posted Date: 3 January 2024

doi: 10.20944/preprints202401.0226.v1

Keywords: tungsten; self-passivating; oxidation resistance; milling time

Preprints.org is a free multidiscipline platform providing preprint service that is dedicated to making early versions of research outputs permanently available and citable. Preprints posted at Preprints.org appear in Web of Science, Crossref, Google Scholar, Scilit, Europe PMC.

Copyright: This is an open access article distributed under the Creative Commons Attribution License which permits unrestricted use, distribution, and reproduction in any medium, provided the original work is properly cited.

Preprints (www.preprints.org) | NOT PEER-REVIEWED | Posted: 3 January 2024 doi:10.20944/preprints202401.0226.v1

Disclaimer/Publisher's Note: The statements, opinions, and data contained in all publications are solely those of the individual author(s) and contributor(s) and not of MDPI and/or the editor(s). MDPI and/or the editor(s) disclaim responsibility for any injury to people or property resulting from any ideas, methods, instructions, or products referred to in the content.

Article

Microstructures and Antioxidation of W Self-Passivating Alloys: Synergistic Effect of Yttrium and Milling Time

Shijie Chen [1], Shirong Zhang [1], Rui Wang [1], Chao Ye [1], Lihong Xue [1,*], Shengming Yin [1], Youwei Yan [1]and Qilai Zhou [2]

[1] State Key Laboratory of Materials Processing and Die and Mould Technology, Huazhong University of Science and Technology, Wuhan 430074, China; shijiechen@hust.edu.cn; zhangshirong@hust.edu.cn; u202210896@hust.edu.cn; yechaoweecl@gmail.com; yinsm@hust.edu.cn; yanyw@hust.edu.cn

[2] School of Materials Science and Engineering, Wuhan University of Technology, Wuhan 430070, China; zhou.qilai@whut.edu.cn

* Correspondence: xuelh@hust.edu.cn

Abstract: Tungsten and its alloys are considered as a key component in high temperature environment. Self-passivating W-Si-xY alloys with different Y contents made from the powders milled for different times were prepared by mechanical alloying (MA) and spark plasma sintering (SPS). Their microstructures and oxidation resistance were investigated. It is found that the oxidation resistance of the alloys with low Y contents (0Y and 2Y) made from 20 h-milled powders is worse than that of the alloys made from 4 h-milled powders. It is because the protective WO_3/SiO_2 composite layer is discontinuous. While the alloys with high Y contents (4Y and 6Y) made from 4 h and 20 h-milled powders show good oxidation resistance. Even, the thickness of the oxide layer of the alloys with 4Y and 6Y made from 20 h-milled powders after oxidation at 1000 °C for 2 h is 84.0 μm and 70.7 μm, less than that made from 4 h-milled powders. This is due to the size and distribution of W_5Si_3, $Y_2Si_2O_7$ aggregates and W-Y-O melt. The synergistic effects of Y contents and milling time on the microstructures and oxidation resistance of the alloys are revealed.

Keywords: tungsten; self-passivating; oxidation resistance; milling time

1. Introduction

Tungsten and its alloys are widely used in various fields such as aerospace [1–3], armor-piercing bullets [4,5] and plasma-facing materials in nuclear fusion reactors [6–8] due to their outstanding properties such as high melting point, high thermal conductivity, low coefficient of thermal expansion, low sputtering yield and low tritium retention yield [9]. However, tungsten also has some disadvantages, one of which is its poor oxidation resistance at high temperatures [10]. It can be oxidized to the volatile WO_3 when the temperature reaches 800 °C and above. As a solution to severe oxidation of pure tungsten at high temperatures, a self-passivating tungsten alloy was proposed [11]. The oxidation resistance mechanism of the self-passivating tungsten alloy is that alloying elements can preferentially form a protective oxide layer on the surface of the alloy in the air environment and prevent further oxidation of W. Up to now, W-Cr-X (X is the third component) and W-Si-X are considered to be the two most promising self-passivating alloys [12–22]. We prepared the W-Si-Y alloy by mechanical alloying (MA) and spark plasma sintering (SPS). It exhibits excellent high-temperature oxidation resistance in the air. After oxidation in air at 1000 °C for 80 h, the oxidation rate of W-Si-Y is only 1.1 % of that of pure W, and the original morphology can still be maintained [22]. Recently, we found that Y contents and milling time have a synergistic effect on microstructures and oxidation resistance of the self-passivating W-Si-xY alloys. The oxidation resistance of the alloys without or with low Y contents prepared by long-time ball milling is worse than that of short-time ball milling. The alloys with high Y contents are just the opposite. The milling time is one key factor of MA process, which can result in different microstructures of the alloys [23–26].

© 2024 by the author(s). Distributed under a Creative Commons CC BY license.

Preprints (www.preprints.org) | NOT PEER-REVIEWED | Posted: 3 January 2024 doi:10.20944/preprints202401.0226.v1

In this work, the synergistic effects of Y contents and milling time on the microstructures and oxidation resistance of W-Si-Y alloys are investigated. The W-Si-Y powders containing different Y contents were milled for 4 h and 20 h, respectively, and later sintered into bulks by SPS. The distribution and size of W_5Si_3 and oxides are investigated, and their effects on oxidation resistance are clarified.

2. Materials and Methods

Elemental powders of W (99.9% purity, 1~5 μm), Si (99.9% purity, ~1 μm) and Y (99.9% purity, ~15 μm) were used to produce W-32Si-xY (x = 0, 2.0, 4.0, 6.0 at. %) alloys. For convenience, the W-32Si-xY compositions were labeled as xY (x represents yttrium content). The MA, SPS and oxidation process are performed according to our previous report [22]. The weighed powders according to the ratio with 5 wt.% of ethanol were mechanically milled in high-energy planetary ball mill under Ar atmosphere at room temperature. Tungsten carbide (WC) balls were adopted. The ball-to-material weight ratio (BPR) was 15:1. The rotation speed was 250 rpm and the milling time was 4 h and 20 h, respectively. SPS process was conducted in the SPS equipment (Sinterland, LABOX-1575, Japan), where powders were consolidated to cylinders at 1550 ℃ for 5 min at 50 MPa. The size of sintered cylinder was 20 mm in diameter and 4 mm in thickness.

The cylinder was processed into cubes with size of 4 × 4 × 4 mm3 by wire-electrode cutting and these cubes were successively ground by 15 μm and 5 μm diamond papers, and finally polished with diamond suspension until six surfaces were mirrored. Oxidation tests were conducted in a high-temperature box resistance furnace with a heating rate 10 ℃ /min from room temperature to 1000 ℃ in air. The cubes were held at 1000 ℃ and last from 0 h to 10 h. The weight of each specimen before and after oxidation was measured by electronic balance with an accuracy of 0.1 mg. Three parallel specimens were adopted in each oxidation testes.

The oxygen content in the powders was measured by the ONH analyzer (G8 Galileo, Germany). The phase composition of the materials was determined by X-ray diffractometer (XRD 7000, Japan), tube voltage 40 kV, tube current 30 mA, the source of the ray is Cu-Kα. Microstructure and composition were observed by scanning electron microscope (SEM, Nova NanoSEM 450, the Netherlands) and energy dispersive spectrometer (EDS).

3. Results and discussion

3.1. Microstructures of the as-prepared powders

Figure 1 shows the SEM images of as-prepared W-Si-xY powders milled for 4 h and 20 h, respectively. With the increase of Y contents, the particle size of the powders decreases and the shape changes from irregular to spherical, indicating that the addition of Y is beneficial to the refinement of W particles. In addition, at the same Y content, the powders milled for 20 h has finer particles than that milled for 4 h.

Figure 2 presents the EDS-mapping of the 2Y and 6Y powders milled for 4 h and 20 h, respectively. It can be seen that the Y distributes unevenly in 2Y and 6Y powders milled for 4 h and there are Y-enriched areas locally (marked with yellow circles). On the contrary, in the case of 20 h milling, the distribution of W, Si and Y in 2Y and 6Y powders is similar, indicating that these elements are uniformly dispersed in the particles.

The XRD patterns of the as-prepared powders milled for 4 h and 20 h are shown in Figure 3. The peaks of W and Si are detected in all the samples. No peaks of Y are observed, probably because of the content of Y is too low to reach the detection limit of XRD.

Preprints (www.preprints.org) | NOT PEER-REVIEWED | Posted: 3 January 2024 doi:10.20944/preprints202401.0226.v1

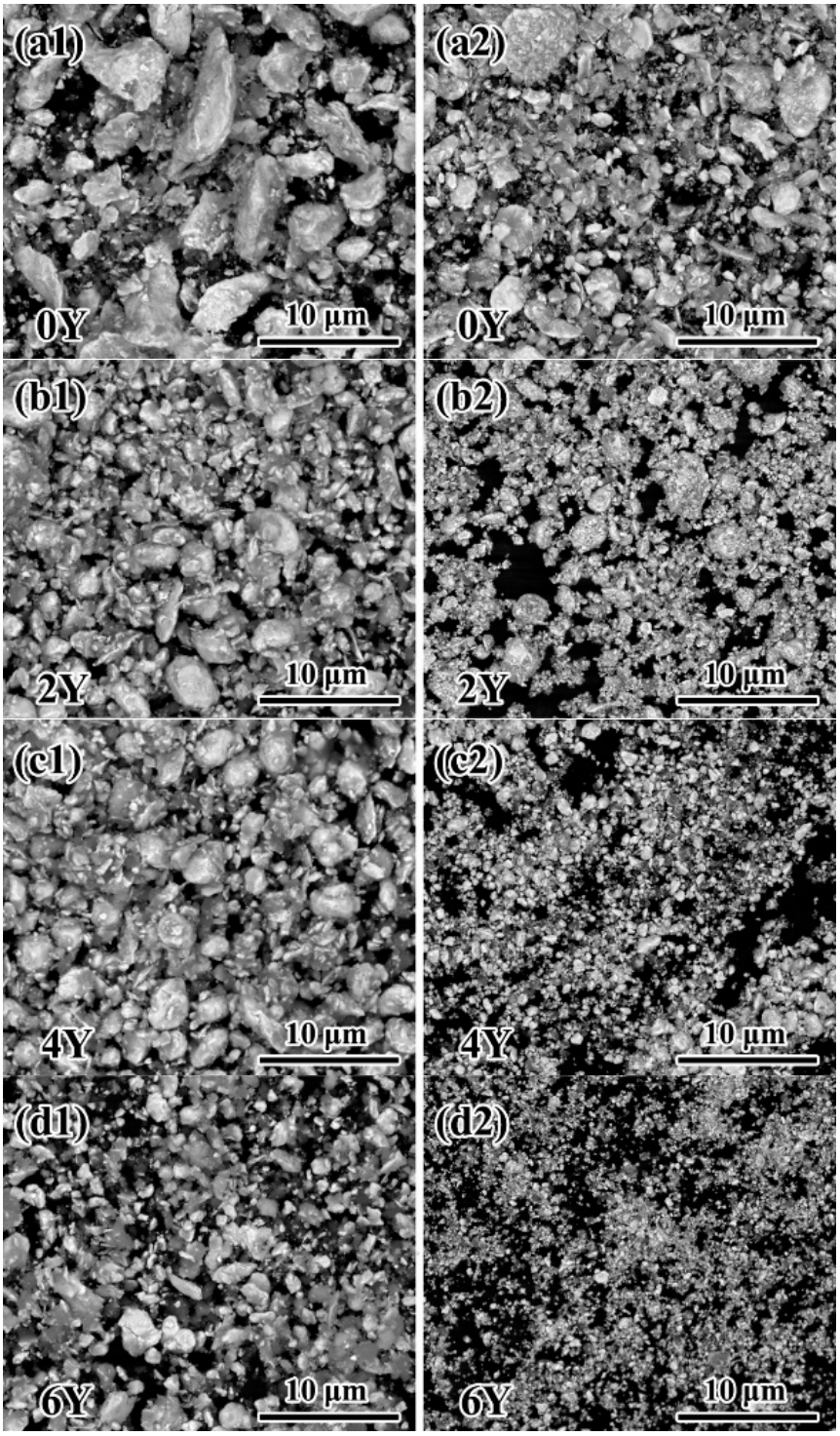

Figure 1. SEM images of as-milled W-Si-xY powders: (a) 0Y, (b) 2Y, (c) 4Y, (d) 6Y; milled for (1) 4 h and (2) 20 h.

Preprints (www.preprints.org) | NOT PEER-REVIEWED | Posted: 3 January 2024 doi:10.20944/preprints202401.0226.v1

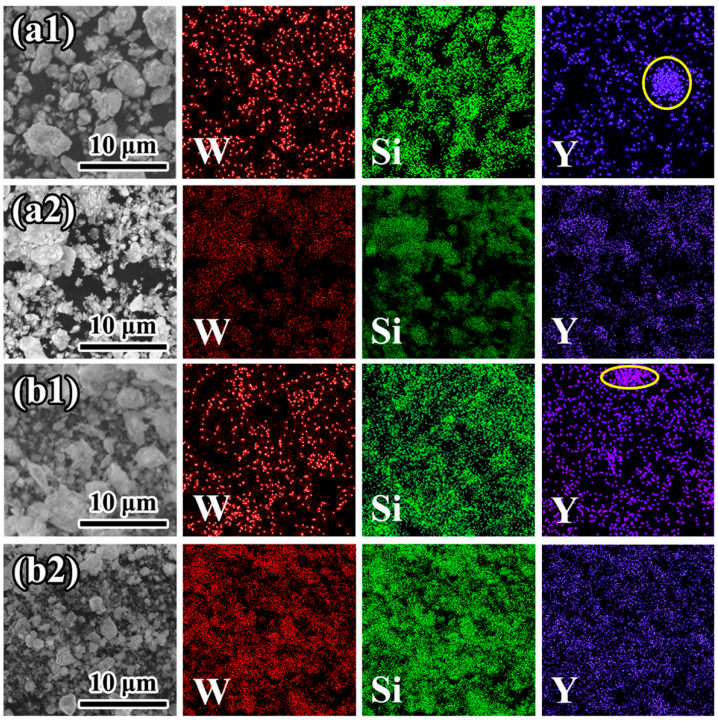

Figure 2. EDS-mapping images of (a) W-Si-2Y and (b) W-Si-6Y powders milled for (1) 4 h and (2) 20 h.

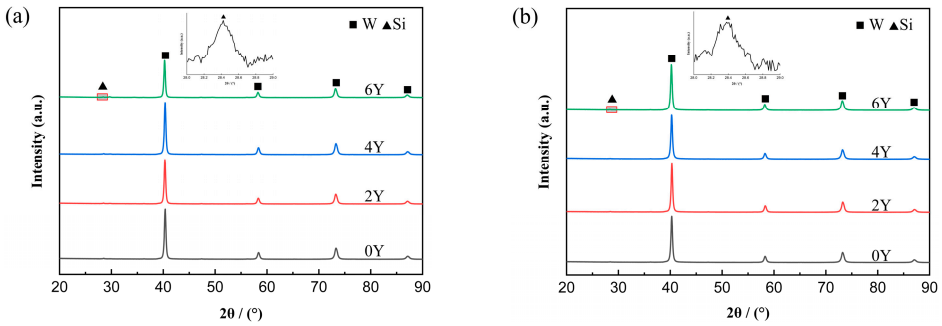

Figure 3. XRD patterns of W-Si-xY powders milled for (a) 4 h and (b) 20 h.

3.2. Microstructures of W-Si-Y sinter alloys

The XRD patterns of W-Si-xY alloys sintered by the powders milling for 4 h and 20 h are shown in Figure 4. These XRD patterns are similar, in which W and W_5Si_3 are the main phases, and a weak SiO_2 diffraction peak is also detected.

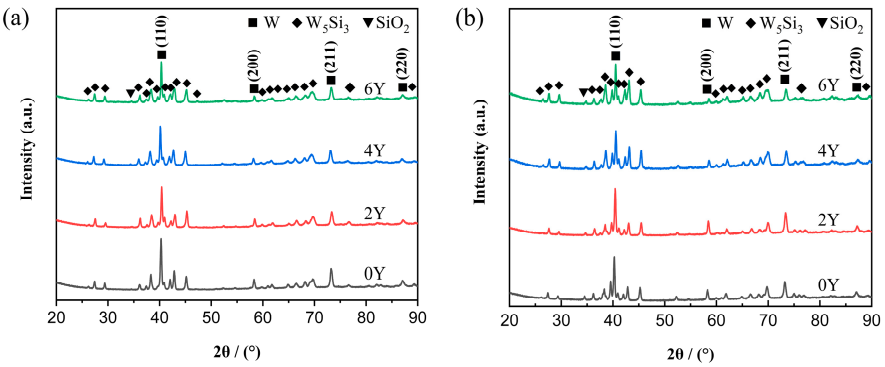

Preprints (www.preprints.org) | NOT PEER-REVIEWED | Posted: 3 January 2024 doi:10.20944/preprints202401.0226.v1

Figure 4. XRD patterns of sintered alloys made from the powders milled for (a) 4 h and (b) 20 h.

The BSE-SEM images of sintered alloys are shown in Figure 5(a)-(d). All the alloys contain black particles (marked as A), gray phase (marked as B) and bright gray phase (marked as C). The details of these phases have been studied [21,22]. According to our research, the gray phase B is W_5Si_3 and bright gray phase C is W. The black particles A are SiO_x (x=1, 2, 3) in the 0Y alloy, while they are mainly SiO_x and a small amount of Y_2O_3 and Y in the 2Y alloy. In the 4Y and 6Y alloys, they are mainly SiO_x, Y_2O_3 and Y-Si-O and a small amount of Y.

The distribution of W_5Si_3 phase plays an essential role in the oxidation resistance of W alloys [27]. It is noticed that the W_5Si_3 is discontinuous in the 0Y and 2Y alloys made from 20 h- milled powders. In the other alloys, the W_5Si_3 phase is continuous. The melting point of silicon is 1410 ℃, which is lower than the sintering temperature (1550 ℃). In addition, long-time milling makes the powders have higher reactivity and adsorb more oxygen. The oxygen content of the powders milled for 20 h is about 21000 ppm, higher than that of the powders milled for 4 h (~12000 ppm). These factors promote the formation of large SiO_2 in the 0Y and 2Y alloys made from 20 h-milled powders, resulting in the separation of the W_5Si_3 phases. However, for the 4Y and 6Y alloys made from 20 h-milled powders, most of the oxygen reacts with Y to form Y-rich oxide particles because Y has higher affinity to O than Si and the content of Y is high. Yttrium has a high melting point (1522 ℃) and is uniformly dispersed in the powder. Therefore, fine Y-rich oxide particles can be formed during the sintering process without splitting the W_5Si_3 phase.

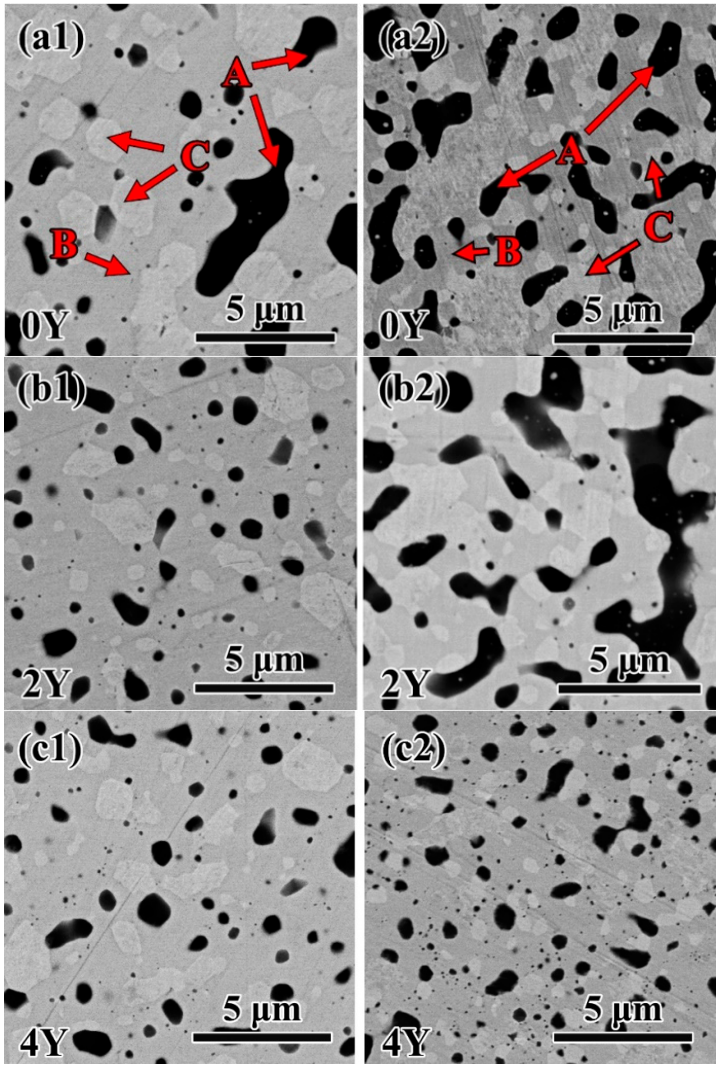

Preprints (www.preprints.org) | NOT PEER-REVIEWED | Posted: 3 January 2024 doi:10.20944/preprints202401.0226.v1

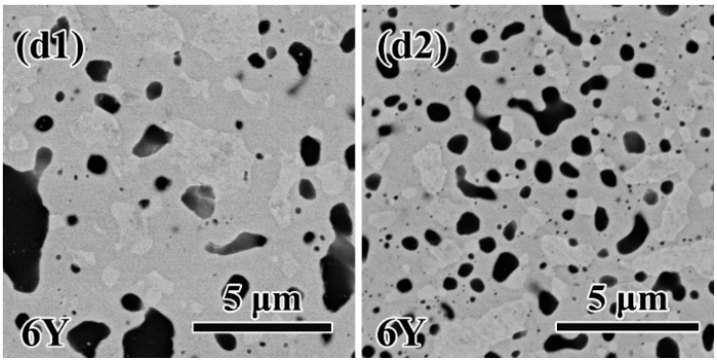

Figure 5. BSE-SEM images of sintered W-Si-xY bulks: (a) 0Y, (b) 2Y, (c) 4Y, (d) 6Y; (1) 4 h milling, (2) 20 h milling.

3.3. Oxidation tests

Figure 6 is the specific weight change of the alloys after oxidation at 1000 ℃ for different times. Except for the 2Y alloy made from 20 h-milled powders, the oxidation weight gain of all other alloys decreases with the addition of Y. In addition, under the same oxidation conditions, the weight gain of the 0Y and 2Y alloys made from 20 h-milled powders is much more than the same composition alloys made from 4 h-milled powders, while the weight gain of the 4Y and 6Y alloys made from 20 h-milled powders is close to or even less than that of the same component alloys made from 4 h-milled powders.

Figure 7 shows the macro-morphology of the alloys after oxidation at 1000 ℃ for different times. Due to the tip thermal effect [28], the oxidation of all alloys is preferentially initiated from the angular edges of the cube. Compared to 0Y and 2Y alloys made from 4 h-milled powders, the oxidation of 0Y and 2Y alloys made from 20 h-milled powders is more serious under the same oxidation conditions. Especially after oxidation for 10 h, their cubic shape is severely damaged. But the appearance of 4Y and 6Y made from 20 h-milled powders is similar to that of the same composition alloys made from 4 h-milled powders, and they all maintain good cubic morphology.

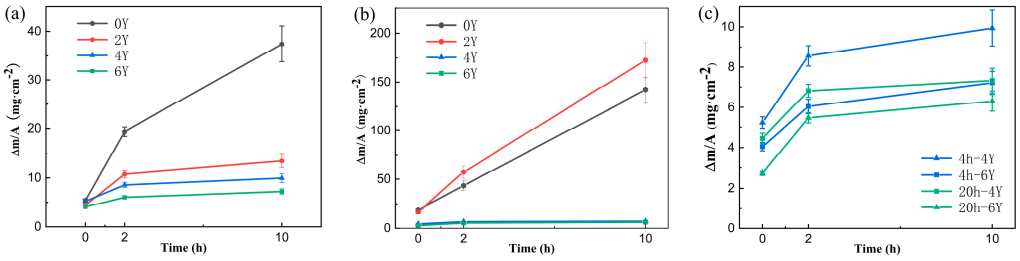

Figure 6. Weight change of the alloys made from the powders milled for (a) 4 h and (b) 20 h after oxidation at 1000 ℃ for different time; (c) the detail of 4Y and 6Y alloys.

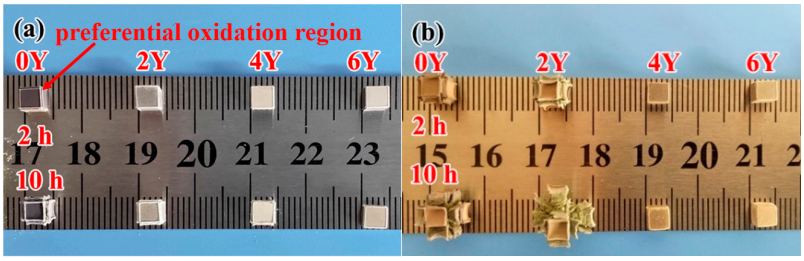

Figure 7. The macro photos of W-Si-xY alloys made from the powders milled for (a) 4 h and (b) 20 h after oxidation at 1000 ℃ for 2 h and 10 h.

Preprints (www.preprints.org) | NOT PEER-REVIEWED | Posted: 3 January 2024 doi:10.20944/preprints202401.0226.v1

3.4. Microstructure of oxidation layer analysis

In order to explain the above phenomenon, the microstructure of the alloys oxidized for 2 h was characterized.

Figure 8 shows the SEM images of the preferential oxidation region (as shown by the arrow in Figure 7) of the alloys oxidized for 2 h. For all the alloys, the oxidation region is composed of porous network layer and some particles. The porous network is confirmed to be WO_3/SiO_2 composite, and the particles are WO_3, SiO_2, W-Fe-O, W-Y-O, etc. [21,22]. Those large black holes are produced by the volatilization of WO_3 or the shedding of some SiO_2 particles. It is noticed that the WO_3/SiO_2 composite layer is discontinuous in 0Y and 2Y alloys made from 20 h-milled powders, but continuous in other alloys. The WO_3/SiO_2 composite is formed by in-situ oxidation of W_5Si_3, so the distribution of the composite is closely related to the W_5Si_3 distribution in the alloy. As mentioned above, in the 0Y and 2 Y alloys made from 20 h-milled powders, W_5Si_3 is discontinuously distributed, so is the WO_3/SiO_2 composite.

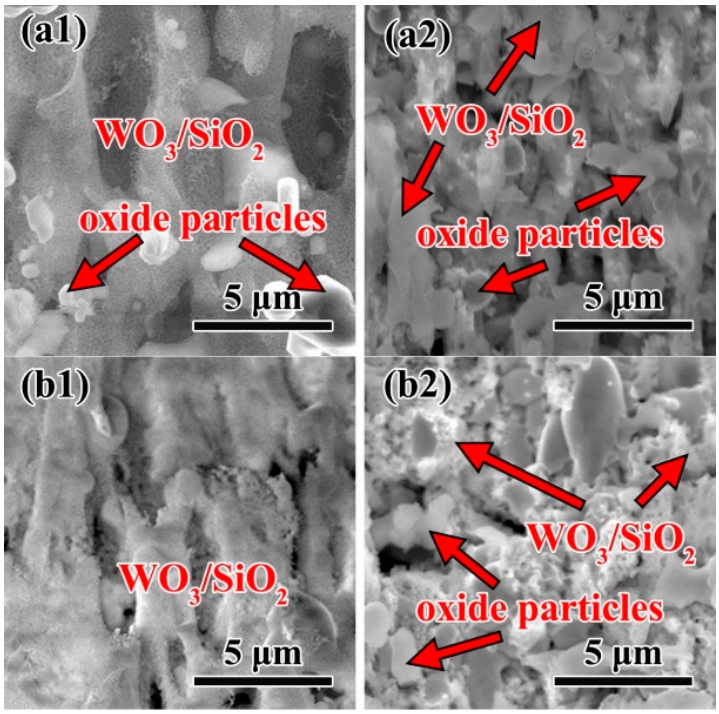

Preprints (www.preprints.org) | NOT PEER-REVIEWED | Posted: 3 January 2024 doi:10.20944/preprints202401.0226.v1

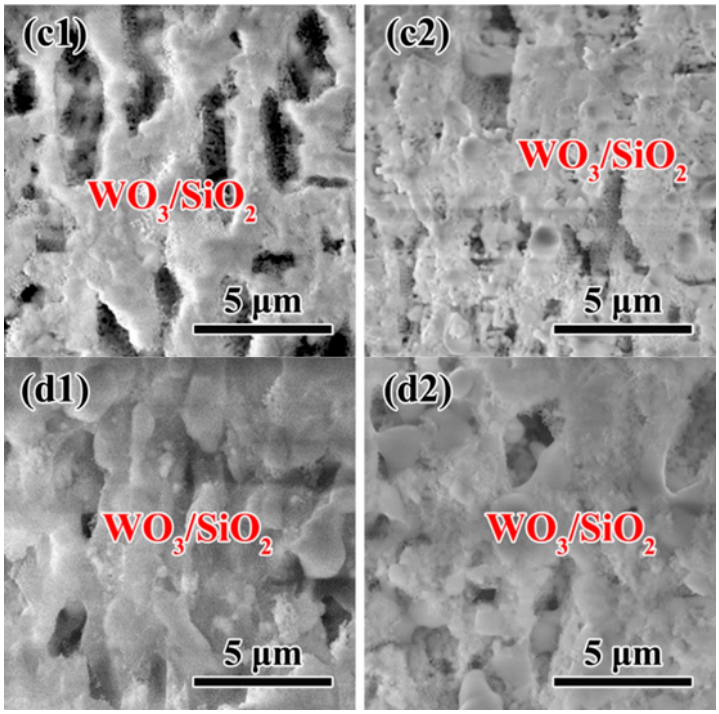

Figure 8. SEM images of the preferential oxidation region of the W-Si-xY alloys oxidized for 2 h: (a) 0Y, (b) 2Y, (c) 4Y, (d) 6Y; (1) 4 h of milling, (2) 20 h of milling.

Figure 9 shows the cross-section BSE-SEM images of the alloys oxidized for 2 h. The thicknesses of the oxide layers in Figure 9 are listed in Table 1. As the Y content increases, the oxide layer thickness decreases. For 0Y and 2Y alloys made from 20 h-milled powders, the oxide layer is much thicker than that made from 4 h-milled powders. For 4Y and 6Y alloys, the opposite is true. In the oxide layer, the oriented bright grey phase is WO_3 and the dark grey phase is WO_3/SiO_2 (the typical images are shown in the inset of Figure 9(b1) and (c2)), which are derived from the in-situ oxidation of W and W_5Si_3 in the alloy, respectively. The black particles in the oxide layer of 0Y alloys are SiO_2. When yttrium is added to the alloy, $Y_2Si_2O_7$ aggregates appear. And the number and size of these aggregates increase with the increase of Y content. And it is found that there is a black edge around the $Y_2Si_2O_7$ aggregates (see the inset of Figure 9(d1)), which is micro crack, this is due to the different thermal expansion coefficient of $Y_2Si_2O_7$ aggregates and WO_3/SiO_2 oxide layer. More detailed information about WO_3, WO_3/SiO_2 and $Y_2Si_2O_7$ aggregates can be found in our report [21,22].

For the 0Y alloy made from 4 h-milled powders, the WO_3/SiO_2 composite oxide is a continuous phase, and no obvious cracks and holes are found at the interface between the alloy and oxide layer; for the same composition alloy made from 20 h-milled powders, the WO_3/SiO_2 composite oxide is a discontinuous phase, which mixed with other oxide particles (the inset of Figure 9(a2)), transverse cracks and porous bands appear at the alloy / oxide layer interface. At the interface between the oxide layer and the alloy, if the rate of new oxide formation is lower than that of oxygen diffuses to the interface, there will be residual oxygen. As the oxidation time increases, more and more residual oxygen will be stored at the interface, causing the region to form a porous zone and separating the oxide layer from the alloy [29,30]. Compared to the 0Y alloy made from 4 h-milled powders, the protective WO_3/SiO_2 phase is a discontinuous phase in the alloy made from 20 h-milled powders, allowing more oxygen to enter the interface at a faster rate. Therefore, it is easier to form cracks and multiple voids at the interface. The microstructure of the oxide layer of 2Y alloy is similar to that of 0Y alloy.

For the 4Y and 6Y alloys made from 4 h and 20 h-milled powders, their WO_3/SiO_2 composite oxide is a continuous phase, and no obvious cracks and holes are found at the interface. In addition, compared with the alloys made from 4 h-milled powders, the $Y_2Si_2O_7$ particles in oxide layer of the

Preprints (www.preprints.org) | NOT PEER-REVIEWED | Posted: 3 January 2024 doi:10.20944/preprints202401.0226.v1

alloys made from 20 h-milled powders are finer, so the cracks formed around them are smaller, and their effect on the oxidation resistance is little.

It is known that the oxide layer of W-Si-6Y alloys has three layers from inside to outside, which are dense WO_3/SiO_2 layer, loose WO_3/SiO_2 layer and W-Y-O molten layer [21]. The molten layer also plays an important role in the oxidation resistance of the alloy, which can slow down the diffusion of oxygen in the environment into the alloy. The molten layer can be observed in 6Y alloys, as shown in Figure 9(d1) and (d2), while it is difficult to see in 2Y and 4Y alloys. For the alloy with low Y content, the W-Y-O melt is to less to form a continuous phase. With the increase of Y content, the melt increases and then forms a continuous phase [21]. Therefore, the oxidation resistance of 6Y alloy is higher than that of 4Y alloy.

According to the above results, it is known that the oxidation resistance of the W alloy is affected by W_5Si_3, W-Y-O molten layer and $Y_2Si_2O_7$ aggregates. For low Y alloys (0Y and 2Y) made from 20 h-milled powders, long-time milling introduces more oxygen and makes silicon have higher reactivity, forming larger SiO_2 particles in the alloys, resulting in the separation of the W_5Si_3 phases. Therefore, the WO_3/SiO_2 composite oxide layer by in situ oxidation of W_5Si_3 is not continuous. So, the oxidation resistance of the 0Y and 2Y alloys prepared by long milling time is worse than that of the alloys prepared by short milling time.

For the high Y alloys (4Y and 6Y) made from 20 h-milled powders, although the oxygen content is higher, most of the oxygen reacts with Y to form small-sized Y-rich oxide particles. Therefore, W_5Si_3 remains continuous, which can provide an effective and continuous oxide protective layer for the alloys. In addition, with the increase of milling time, Y is refined and dispersed uniformly, so the $Y_2Si_2O_7$ particles formed by oxidation are small, which have little adverse effects on the oxidation resistance of the alloy. Therefore, the 4Y and 6Y alloys made from 20 h-milled powders has better oxidation resistance than the same composition alloys made from 4 h-milled powders.

In addition, for the alloys with high Y content, a continuous W-Y-O melt can be formed on the outmost surface to further improve the oxidation resistance.

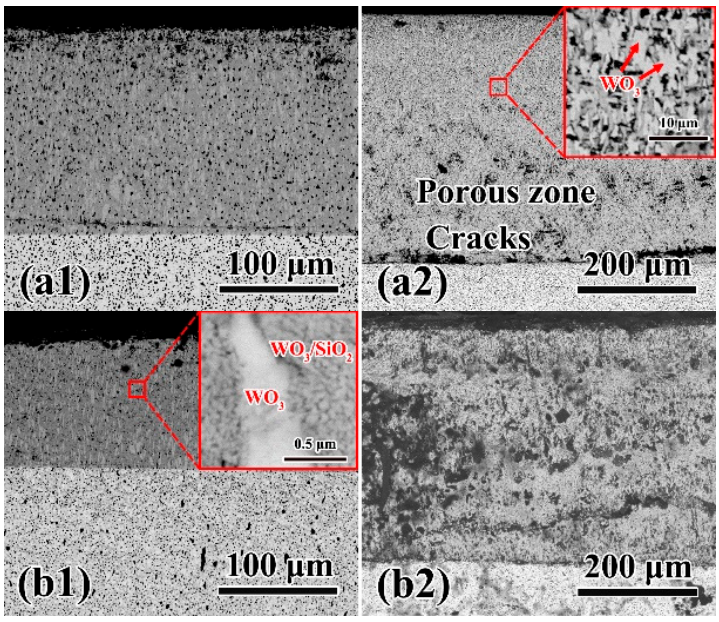

Preprints (www.preprints.org) | NOT PEER-REVIEWED | Posted: 3 January 2024 doi:10.20944/preprints202401.0226.v1

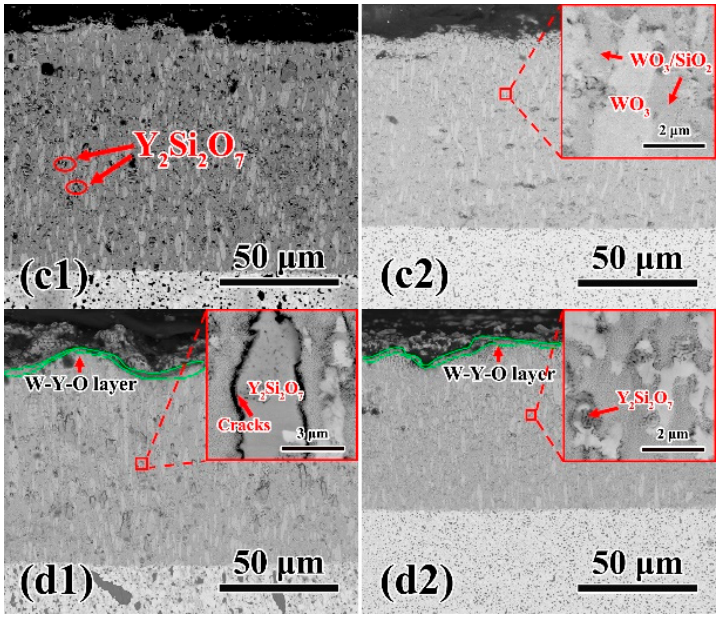

Figure 9. BSE-SEM images of the cross-sections of W-Si-xY samples after oxidation at 1000 ℃ for 2 h: (a) 0Y, (b) 2Y, (c) 4Y, (d) 6Y; (1) 4 h of milling, (2) 20 h of milling.

Table 1. The oxide layer thickness of the oxidized W-Si-xY alloys in Figure 9.

Alloys	Thickness(μm)	
	4 h of milling	20 h of milling
W-32Si	173.6	413.8
W-32Si-2Y	108.1	395.7
W-32Si-4Y	104.7	84.0
W-32Si-6Y	83.6	70.7

4. Conclusions

The synergistic effects of Y contents and milling time on the microstructure and oxidation resistance of W-Si-Y alloys was investigated. It is found that the milling time affects the distribution of W_5Si_3 and the size of $Y_2Si_2O_7$ aggregates, which are the key factors of oxidation resistance.

For the 0Y and 2Y alloys, the oxidation resistance of the alloys made from 20 h-milled powders is worse than that of the alloys made from 4 h-milled powders. It is because Si has higher reactivity by longer milling time and form larger and more SiO_2 particles in the alloys, resulting in the separation of the W_5Si_3 phases. The WO_3 / SiO_2 composite oxide layer formed by in-situ oxidation of W_5Si_3 is also discontinuous, which cannot effectively prevent oxygen from entering the alloy.

For the 4Y and 6Y alloys, the oxidation resistance of the alloys made from 20 h-milled powders is better than that of the alloys made from 4 h-milled powders. The main reasons are that most of the oxygen reacts with Y to form small-sized Y-rich oxide particles. Therefore, W_5Si_3 remains continuous, which can provide an effective and continuous WO_3 / SiO_2 oxide protective layer for the alloys. In addition, the $Y_2Si_2O_7$ particles formed by oxidation in the alloy made form the powders by long time milling are smaller than that prepared by short time milling, which have little adverse effects on the oxidation resistance of the alloy.

Author Contributions: Conceptualization, Chao Ye and Lihong Xue; Funding acquisition, Youwei Yan and Qilai Zhou; Investigation, Shijie Chen, Shirong Zhang and Rui Wang; Methodology, Shijie Chen and Lihong Xue; Project administration, Lihong Xue; Resources, Shengming Yin, Youwei Yan and Qilai Zhou; Supervision, Lihong Xue and Youwei Yan; Visualization, Shijie Chen; Writing – original draft, Shijie Chen and Lihong Xue; Writing – review & editing, Shijie Chen and Shengming Yin.

Preprints (www.preprints.org) | NOT PEER-REVIEWED | Posted: 3 January 2024 doi:10.20944/preprints202401.0226.v1

Funding: This research was funded by the National MCF Energy R&D Program, grant number 2018YFE0306104 and State Key Laboratory of Materials Processing and Die & Mould Technology, Huazhong University of Science and Technology, grant number P2023-024.

Data Availability Statement: Data Availability Statement: The data used to support the findings of this study are available from the corresponding author upon request.

Acknowledgments: The authors thank the help from analytical and testing center in Huazhong University of Science and Technology.

Conflicts of Interest: The authors declare no conflict of interest.

References

1. Wang, Y.J.; Peng, H.X; Zhou, Y.; Song, G.M. Influence of ZrC content on the elevated temperature tensile properties of ZrCp/W composites. *Materials Science and Engineering: A* **2011**, *528*, 1805-1811. https://doi.org/10.1016/j.msea.2010.11.029.
2. Kharchenko, V.; Bukhanovskii, V. High-temperature strength of refractory metals, alloys and composite materials based on them. *Strength of Materials* **2012**, *44*, 512-517. https://doi.org/10.1007/s11223-012-9417-y.
3. Zheng, X.; Bai, R.; Wang, D.H.; Cai, X.M.; Wang, F.; Xia, X.M.; Yu, L.J. Research Development of Refractory Metal Materials Used in the Field of Aerospace. *Rare Metal Materials and Engineering* **2011**, *40*, 1871-1875.
4. Kolmakov, A; Bannykh, I.; Antipov, V.; Vinogradov, L.; Sevost'yanov, M. Materials for bullet cores. *Advanced Materials and Technologies*, **2021**, 4, 351-362. https://doi.org/10.1134/S0036029521040133.
5. Benedetto, G.; Matteis, P; Scavino, G. Impact behavior and ballistic efficiency of armor-piercing projectiles with tool steel cores. *International Journal of Impact Engineering* **2018**, 115, 10-18. https://doi.org/10.1016/j.ijimpeng.2017.12.021.
6. Pitts, R.; Bonnin, X.; Escourbiac, F.; Frerichs, H.; Gunn, J.; Hirai, T.; Kukushkin, A.; Kaveeva, E.; Miller, M.; Moulton, D.; Rozhansky, V.; Senichenkov, I.; Sytova, E.; Schmitz, O.; Stangeby, P.; Temmerman, G; Veselova, I.; Wiesen, S. Physics basis for the first ITER tungsten divertor. *Nuclear Materials and Energy*. **2019**, 20, 100696. https://doi.org/10.1016/j.nme.2019.100696.
7. Cheng, Z.Y.; Sun, J.R.; Gao, X; Wang, Y.Y.; Cui, J.H.; Wang, T.; Chang, H.L. Irradiation effects in high-entropy alloys and their applications. *Journal of Alloys and Compounds*. **2023**, 930, 166768. https://doi.org/10.1016/j.jallcom.2022.166768.
8. Bucalossi, J.; Achard, J.; Agullo, O.; Alarcon, T.; Allegretti, L.; Ancher, H.; Antar, G.; Antusch, S.; Anzallo, V.; Arnas, C . Operating a full tungsten actively cooled tokamak: overview of WEST first phase of operation. *Nuclear Fusion*. **2023**; 62; 042007. https://doi.org/10.1088/1741-4326/ac2525.
9. Philipps, V. Tungsten as material for plasma-facing components in fusion devices. *Journal of Nuclear Materials*. **2011**, 415, S2-S9. https://doi.org/10.1016/j.jnucmat.2011.01.110.
10. Habainy, J.; Iyengar, S.; Surreddi, K.; Lee, Y.; Dai, Y. Formation of oxide layers on tungsten at low oxygen partial pressures. *Journal of Nuclear Materials*. **2018**, 506, 26-34. https://doi.org/10.1016/j.jnucmat.2017.12.018.
11. Koch, F.; Bolt, H. Self-passivating W-based alloys as plasma facing material for nuclear fusion. *Physica Scripta*. **2007**, T128, 100-105. https://doi.org/10.1088/0031-8949/2007/T128/020.
12. Wegener, T.; Klein, F.; Litnovsky, A.; Rasinski, M.; Brinkmann, J.; Koch, F.; Linsmeier, C. Development of yttrium-containing self-passivating tungsten alloys for future fusion power plants. *Nuclear Materials and Energy*. **2016**, 9, 394-398. https://doi.org/10.1016/j.nme.2016.07.011.
13. Tan, Y.; Klein, F.; Litnovsky, A.; Wegener, T.; Schmitz, J.; Linsmeier, C.; Coenen, J.; Breuer, U.; Rasinski, M.; Li, P.; Luo, L.M.; Wu, Y.C. Evaluation of the high temperature oxidation of W-Cr-Zr self-passivating alloys. *Corrosion Science*. **2019**, 147, 201-211. https://doi.org/10.1016/j.corsci.2018.11.022.
14. Klein, F.; Gilbert, M.; Litnovsky, A.; Gonzalez-Julian, J.; Weckauf, S.; Wegener, T.; Schmitz, J.; Linsmeier, C.; Bram, M.; Coenen, J. Tungsten–chromium–yttrium alloys as first wall armor material: Yttrium concentration, oxygen content and transmutation elements. *Fusion Engineering and Design*. **2020**, 158, 111667. https://doi.org/10.1016/j.fusengdes.2020.111667.
15. Sal, E.; Garcia-Rosales, C.; Schlueter, K.; Hunger, K.; Gago, M.; Wirtz, M.; Calvo, A.; Andueza, I.; Neu, R.; Pintsuk, G. Microstructure. oxidation behaviour and thermal shock resistance of self-passivating W-Cr-Y-Zr alloys. *Nuclear Materials and Energy*. **2020**, 24, 100770. https://doi.org/10.1016/j.nme.2020.100770.
16. Wang, W.J.; Tan, X.Y.; Liu, J.Q.; Chen, X.; Wu, M.; Luo, L.M.; Zhu, X.Y.; Chen, H.Y.; Mao, Y.R.; Litnovsky, A.; Coenen, J.W.; Linsmeier, Ch.; Wu, Y.C. The influence of heating rate on W-Cr-Zr alloy densification process and microstructure evolution during spark plasma sintering. *Powder Technology*. **2020**, 370, 9-18. https://doi.org/10.1016/j.powtec.2020.05.020.
17. de Prado, J.; Sal, E.; Sanchez, M.; Garcia-Rosales, C.; Urena, A. Microstructural and mechanical characterization of self-passivating W-Eurofer joints processed by brazing technique. *Fusion Engineering and Design*. **2021**, 169, 112496. https://doi.org/10.1016/j.fusengdes.2021.112496.

Preprints (www.preprints.org) | NOT PEER-REVIEWED | Posted: 3 January 2024 doi:10.20944/preprints202401.0226.v1

18. Litnovsky, A.; Klein, F.; Tan, X.; Ertmer, J.; Coenen, J.; Linsmeier, C.; Gonzalez-Julian, J.; Bram, M.; Povstugar, I.; Morgan, T.; Gasparyan, Y.; Suchkov, A.; Bachurina, D.; Nguyen-Manh, D.; Gilbert, M.; Sobieraj, D.; Wrobel, J.; Tejado, E.; Matejicek, J.; Zoz, H.; Benz, H.; Bittner, P.; Reuban, A. Advanced self-passivating alloys for an application under extreme conditions. *Metals*. **2021**, 11, 1255. https://doi.org/10.3390/met11081255.
19. Wang, J.Z.; Wu, T.; Tian, L.H.; Lin, N.M.; Wang, Z.X.; Qin, L.; Wu, Y.C. Preparation of self-passivation W-Cr-Y alloy layer and its oxidation resistance. *Heat Treatment of Metals*. **2023**, 48, 202-206. https://doi.org/10.13251/j.issn.0254-6051.2023.01.036.
20. Liu, W.; Di, J.; Xue, L.H.; Li, H.P.; Oya, Y.; Yan, Y.W. Phase evolution progress and properties of W-Si composites prepared by spark plasma sintering. *Journal of Alloys and Compounds*. **2018**, 766, 739-747. https://doi.org/10.1016/j.jallcom.2018.07.038.
21. Liu, W.; Di, J.; Zhang, W.X.; Xue, L.H.; Yan, Y.W. Oxidation resistance behavior of smart W-Si bulk composites. *Corrosion Science*. **2020**, 163, 108222. https://doi.org/10.1016/j.corsci.2019.108222.
22. Yi, G.Q.; Liu, W.; Ye, C.; Xue, L.H.; Yan, Y.W. A self-passivating W-Si-Y alloy: Microstructure and oxidation resistance behavior at high temperatures. *Corrosion Science*. **2021**, 192, 109820. https://doi.org/10.1016/j.corsci.2021.109820.
23. López-Ruiz, P.; Koch, F.; Ordás, N.; Lindig, S.; García-Rosales, C. Manufacturing of self-passivating W-Cr-Si alloys by mechanical alloying and HIP. *Fusion Engineering and Design*. **2011**, 86, 1719-1723. https://doi.org/10.1016/j.fusengdes.2011.03.107.
24. López-Ruiz, P.; Ordás, N.; Lindig, S.; Koch, F.; Iturriza, I.; García-Rosales, C. Self-passivating bulk tungsten-based alloys manufactured by powder metallurgy. *Physica Scripta*. **2011**, T145, 014018. https://doi.org/10.1088/0031-8949/2011/T145/014018.
25. Chen, B.; Shen, J.; Ye, X.; Jia, L.; Li, S.; Umeda, J.; Takahashi, M.; Kondoh, K. Length effect of carbon nanotubes on the strengthening mechanisms in metal matrix composites. *Acta Materialia*. **2017**, 140, 317-325. https://doi.org/10.1016/j.actamat.2017.08.048.
26. Han, Z.G.; Zhai, T.T.; Yuan, Z.M.; Liu, F.C.; Feng, D.C.; Sun, H.; Zhang, Y.H. Improved Electrochemical Performances of Ti-Fe Based Alloys by Mechanical Milling. *International Journal of Electrochemical Science*. **2023**, 17, 221285. https://doi.org/10.20964/2022.12.81.
27. Liu, W.; Ye, C.; Xue, L.H.; Zhang, W.; Yan, Y.W. A self-passivating tungsten bulk composite: Effects of silicon on its oxidation resistance. *International Journal of Refractory Metals and Hard Materials*. **2021**, 100, 105631. https://doi.org/10.1016/j.ijrmhm.2021.105631.
28. Gulbransen, E.A.; Andrew, K.F. Kinetics of the oxidation of pure tungsten from 500° to 1300 ◦C. *Journal of the Electrochemical Society*. **1960,** 107, 619–628. https://doi.org/10.1149/1.2427787.
29. Telu, S.; Patra, A.; Sankaranarayana, M.; Mitra, R.; Pabi, S. Microstructure and cyclic oxidation behavior of W-Cr alloys prepared by sintering of mechanically alloyed nanocrystalline powders. *International Journal of Refractory Metals & Hard Materials*. **2013**, 36, 191–203. https://doi.org/10.1016/j.ijrmhm.2012.08.015.
30. Telu, S.; Mitra, R.; Pabi, S. Effect of Y2O3 Addition on Oxidation Behavior of W-Cr Alloys. *Metallurgical and Materials Transactions A-Physical Metallurgy and Materials Science*. **2015**, 46A, 5909-5919. https://doi.org/10.1007/s11661-015-3166-z.

Disclaimer/Publisher's Note: The statements, opinions and data contained in all publications are solely those of the individual author(s) and contributor(s) and not of MDPI and/or the editor(s). MDPI and/or the editor(s) disclaim responsibility for any injury to people or property resulting from any ideas, methods, instructions or products referred to in the content.